JIT Mahasarakham University, Thailand
http://jit.it.msu.ac.th

Journal of Applied Informatics and Technology, 6 (1), 33-51

Research Article

Modeling Deep Feature for Lung Disease Classification in Chest X-ray Images

Ei Ei Khaing[1,*], Thu Zar Aung[2]

[1] Faculty of Computer System and Technologies, University of Computer Studies (Taungoo), Myanmar
[2] University of Technology (Yatanarpon Cyber City), PyinOoLwin, Myanmar
* Corresponding Author: Ei Ei Khaing, eekhaingct@gmail.com

Received:
10 July 2023
Revised:
7 September 2023
Accepted:
14 October 2023

Keywords:

CNN, AlexNet, LSTM, SVM Classifier, Lung Disease, Classifier Performance

Abstract: An accurate method of diagnosis is needed as lung disease spreads around the globe. Since COVID-19 spreads so quickly, diagnosing lung disease can be challenging for medical professionals. Clinical diagnosis is distinguished by the accuracy of its diagnosis and treatment because they typically depend on a doctor's skill and knowledge. This is the most challenging aspect of diagnosing COVID-19 and pneumonia patients. Therefore, for the time being, the deep learning technology's major objective is to create a way to detect lung problems early and stop the virus from spreading quickly. The lung disease classification system offers a categorization framework for a challenging image analysis task in the medical field, where chest X-ray images are assessed. The pre-trained Alex Net was utilized to generate the feature map that was taken from the x-ray image. The LSTM model models the extracted feature map to extract a feature vector for a Support Vector Machine (SVM) classifier to categorize lung diseases. In the method of convolutional neural network (CNN) classification, a large number of layers, values, thresholds, and parameters are required to be defined for classification. Since the pre-trained Alex Net is used in our proposed framework, the parameter values for CNN don't need to be defined, reducing processing time effectively. This paper proposes the modeling of feature maps using LSTM and the application of machine learning techniques gave the accuracy of 98.8% for the categorization of lung diseases

in the form of 10-fold cross validation. Three diseases are distinguished in the proposed framework: normal, viral pneumonia, and COVID-19. In experiments, accuracy, true positive, false negative, positive predictive, and false discovery rates were used to evaluate classifier performance.

1. Introduction

Object recognition is a type of vision technology used to categorize things in photographs or video data. Deep learning and machine learning algorithms produce outcomes for object recognition. Diagnosis is a crucial part of a doctor's job, and it requires competent evaluation skills. Early identification of the disease's name allows for a straightforward diagnosis. Due to the rapid advancement of intelligent healthcare systems and the rise in COVID-19 cases, object identification is essential in the medical sector.

Ouyang *et al.* (2020) proposed the use of CT scans, and a dual-sampling attention network was created to quickly identify COVID-19. When establishing diagnosis determinations, it was advised to concentrate on disease areas inside the lungs using an online care system with a 3D CNN. A CNN, SVM, and Sobel filter fusion were recommended for the detection of COVID-19 utilizing X-ray images. A new dataset of X-ray images was obtained and processed using a high-pass filter that used a Sobel filter to extract the image contours. Sharifrazi *et al.* (2021) proposed a fusion classification system in which the loading of the images into a CNN deep transfer learning, and an SVM classifier employing a ten-fold validation set approach was used to classify the images. The performance of CNN was improved by the Sobel filter and CNN-SVM combo.

Wang *et al.* (2020) implemented deep features and machine learning classification to provide a novel and efficient diagnostic method which utilized a thorough diagnostic methodology. The effectiveness of the recommended approach is demonstrated by the fact that it was evaluated on two datasets and performed remarkably well on each of them. When compared to the baseline technique, the diagnostic effectiveness of Xception and SVM were statistically significant. In the work of Tomar & Agarwal (2015), the extracted deep features were injected into machine learning approaches and utilized to introduce the COVID-19 and TB classification methods from X-ray pictures. This was done to address computational challenges in image identification and health-care smart systems. Machine learning approaches were utilized to choose the proper attributes and forecast COVID-19 patients after the features were developed. For illness and lung information, all pictures were normalized for field fragmentation, from which location-specific characteristics were then extracted. With the introduction of the infection-size-aware random forest (iSARF) approach, subjects were automatically divided into groups based on the sizes of the infected carcinomas, and random forests were then used to categorize each group.

Mohammad-Rahimi *et. al.* (2021) proposed research into illness screening using automated machine learning which remains a primary objective despite several studies examining conventional CT radiological signals in COVID-19 patients to direct medical therapy. In medicine, a misdiagnosis has the potential to be fatal. Recent medical investigations have found that interpreting CT images incorrectly is a major cause of pharmacological errors that harm health. One of the biggest problems with this treatment is the growing radioactive contamination that patients accumulate as a result of the extensive use of CT. Medical professionals have effectively used digital image processing and machine learning techniques to solve these medical issues. In order to facilitate image classification algorithms, CNN trains characteristics with fewer dimensions and abstract concepts. The main difficulties faced during CNN model instruction are excessive fitting, class discrepancy, and rising rates. The computational cost and speed of the model may be impacted by these issues. Deep transfer learning is a superior method for tackling these CNN feature extraction problems. It also has the ability to extract features without a GPU.

Kanjanasurat *et al.* (2023) employed the combination of CNNs and RNNs to enhance the classification outcome. This decision was made due to the CNN's proficiency in extracting features efficiently, albeit lacking connectivity between nodes within the same layer. On the other hand, the RNN possesses the ability to analyze dependencies and continuity in preceding information, thereby facilitating pattern recognition based on the extracted features. The study aimed to determine the optimal combination of CNN architectures, including VGG19, ResNet152V2, and DenseNet121, with a recurrent neural network (RNN) variant that includes long-short-term memory (LSTM) and gated recurrent units (GRU). The objective was to identify the most effective CNN-RNN architecture in terms of performance outcomes. The experimental results did not include a comparative analysis of the performance of different CNNs when paired with various RNN versions. The integration architecture of CNN and RNN models, which rely on high-resource devices, necessitates the utilization of GPUs and a minimum of 16 GB of RAM for model training.

In the work of Xia *et al.* (2023), instead of utilizing authentic chest X-rays and CT scan images, the system incorporated images generated through diverse radionics methodologies to train CNNs for the purpose of diagnosing COVID-19. The radionics methodology employed various image processing techniques, including the gray-level run length matrix, gray-level covariance matrix, and discrete wavelet transform, to get modified versions of radiomic images for the purpose of training CNNs. The segmentation of the lung region from CT scan images was performed using a pre-trained U-Net model. Subsequently, ACE2-RGF was utilized as a surrogate biomarker to assess ACE2 expression. The AUC feature selection approach was employed to

identify the optimal features for representing lung information in the categorization of lung diseases.

To prevent patient fatalities, it is necessary to forecast both chronic pulmonary illnesses and COVID-19 infections, as explained by new methods. In order to answer the aforementioned concerns and accomplish multi-class classification from online public repositories, Bhosale & Patnaik (2023) concentrated on finding datasets relevant to chronic pulmonary disorders using COVID-19. The ulDi-COVID framework was devised by integrating various DL model snapshots to classify lung illnesses. The utilization of the framework has played a crucial role in the identification of COVID-19 cases among individuals with chronic lung diseases as well as in the generation of CXI through the implementation of the SSE approach. A diversity of transfer-learning models, such as VGG16, ResNet152V2, VGG19, DenseNet169, DenseNet201, NAS Net Mobile, ResNet50, and MobileNetV2, have been employed in training for the purpose of chronic lung diseases and COVID-19 cases in the context of CXI.

Alshmrani *et al.* (2023) deployed a pre-trained model, VGG19, which was afterward accompanied by the use of three blocks of a CNN for the purpose of feature extraction. Additionally, a fully connected network was employed to carry out the classification task. The proposed intelligent systems used a feedback mechanism to enhance their performance iteratively. The task of analyzing substantial volumes of clinical data is a significant challenge. The use of data mining, artificial intelligence (AI), and deep learning methodologies proves advantageous in the advancement of intelligent computer-aided diagnostic systems, enabling precise diagnosis of diverse illnesses and medical situations.

Khan *et al.* (2023a) proposed a deep dual-patch attention mechanism (D^2PAM) to predict epileptic seizures. The proposed methodology for the processing of brain signals aims to transform the impulses into discrete units of data. The combination of Deep Neural Network (DNN) and D^2PAM has proven to be effective in pre-ictal classification. This approach facilitates the identification of patients who are at a higher risk of experiencing epileptic seizures, even when there are variations among them. The value of the projected model for distinguishing between seizure and healthy signals is assessed using EEG signals. Bonn University, a public and open-source website, provided the dataset for their research. Khan *et al.* (2023b) described a method for diagnosing the source of pneumonia, such as COVID-19 or other infections, from radiography pictures by employing three Convolution Neural Networks (CNNs). The dataset of healthy and pneumonia-infected individuals was compiled using Kaggle and other online resources, as well as pulmonologists in Pakistan. Based on the intricacy of the data, Kujur *et al.* (2022) explored the dependence of brain MRI on multiple CNN predictive models for brain tumors and Alzheimer's disease. Four

CNN models were implemented using the methodologies presented on two brain MRI image datasets to compare the classifiers' performance over five-fold cross-validation.

Vishnoi *et al.* (2023) employed a deep learning model to address the challenges associated with storage and processing resources in the identification of plant diseases using leaf photos. This study presented the development of a convolutional neural network (CNN) with a reduced number of layers, resulting in a decreased computational load. The PlantVillage dataset was utilized for the purpose of detecting Scab, Black rot, and Cedar rust diseases in apple leaves.

In this research, we provide a comprehensive framework for lung disease classification. The proposed approach uses machine learning techniques, feature modeling, and deep transfer learning approaches. During the research that was carried out, a model called a long-short-term memory (LSTM) was utilized for the purpose of processing deep features. After that, it was normalized to generate a feature vector that could be effectively utilized in machine-learning actions. The main contributions of the proposed system are as follows:

- In convolutional neural networks, convolution and pooling layers, and thus the goal is to get a feature map of an image.
- The CNN-based feature is modeled by LSTM to form a feature vector to represent image information.
- The extracted feature vector is trained by a Support Vector Machines (SVM) classifier to get efficient and effective training time for better results.

The paper covered various topics, including an introduction, a proposed theoretical framework, a dataset with related experimental findings, and a conclusion.

2. Materials and Methods

2.1 Lung disease classification

The COVID-19 illness categorization system is a crucial component of healthcare advancement and has an effect on global healthcare. If a COVID-19-positive patient is found at an early stage, associated diseases can be swiftly identified and treated. The manual monitoring of COVID-19-positive cases is exceedingly challenging and necessitates a lot of physical labor, medical knowledge, and lengthy processing periods. A good feature is crucial in computer vision and image processing to accurately capture the traits of a typical image with a limited set of parameters. The suggested system seeks to provide a system that uses image processing methods, deep features, and the SVM algorithm to find COVID-19 in X-ray pictures of the lungs. The suggested system consists of four key steps, as shown in Figure 1.

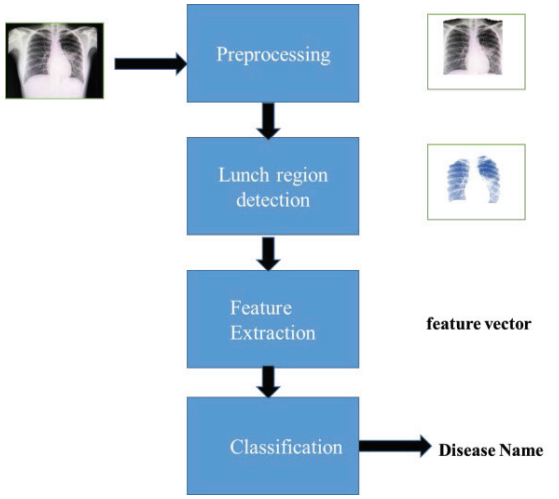

Figure 1. Scheme of Chest X-ray Image Classification

2.2 Preprocessing step

The input of the preprocessing step is chest X-ray images and the output is masked images where lungs regions are extracted using image processing methods as follows.

- **Color thresholding**. The gray level thresholding method is used as the foundation for the color thresholding approach, with a few minor modifications. The Otsu thresholding method is used in which the observation of gray scale value in lung regions generates the threshold value. The grey level of color is taken when the value of level is greater than or equal to threshold value.
- **Morphological operation**. The resulting image obtained through the process of color thresholding exhibits the presence of small regions with holes in both the lung area and the backdrop. Therefore, to eliminate these small zones, a morphological operation known as the open method is employed in which the connectivity value is 8. This method involves the removal of all related objects from a binary image that contain fewer than a specified number of pixels. The result of this procedure is the elimination of diminutive entities from a binary image.
- **Region filling**. The method that is referred to as region filling is applied to complete the image that was produced because of the morphological process by filling in the blank regions that were left over. The process of filling in portions of an image that are missing data is referred to as region filling, and it is done with the goal of filling any holes that may exist.

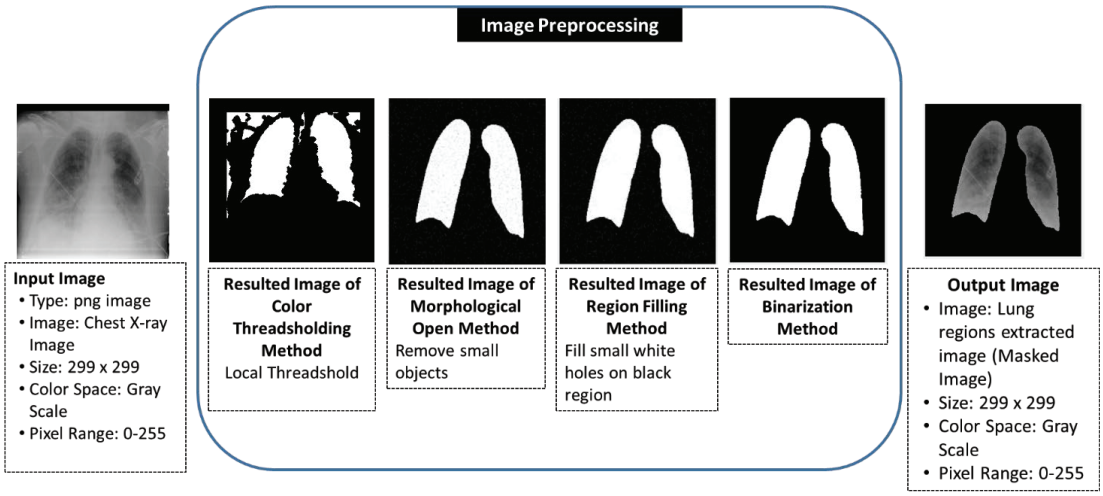

Figure 2. Preprocessing Step of Chest X-ray Image

- **Binarization**. A picture is binarized by changing each pixel's value to '0' or '1' based on whether it is lower than or greater than a threshold value, respectively.
- **Mask**. Image masking is used to describe **hiding and revealing some parts of an image**. Finally, mask the binarized image to obtain a clear mask X-ray image. The visualization of image pre-processing is shown in the following Figure 2.

2.3 Feature extraction step

The models that the previous network learned to extract the important features from fresh data were then used in feature extraction in neural networks. The newly created classifier, which has already been trained from scratch, is then applied to the features. In the case of convolutional networks, feature extraction entails taking the convolutional base of the previously trained network, feeding fresh input through it, and then training a new classifier on top of the network's output. The convolution base of the model refers to the first portion of conv-nets, which includes a number of pooling and convolution layers before connecting with a classifier. Convolutional bases are typically utilized for feature extraction since they are more versatile than tightly coupled layers.

Regardless of the computer-vision problem or any other problem, the feature maps of the network are the presence maps of generic ideas across an image. It is not possible to extract features from tightly linked layers because they lose the ability to explain the position of objects in the input picture. Convolutional feature maps continue to represent the location of objects in densely connected layers. The extracted feature maps can be utilized to enhance an image's deep characteristics. There are two main feature extraction steps in our proposed system. The first step is the generation of a feature map

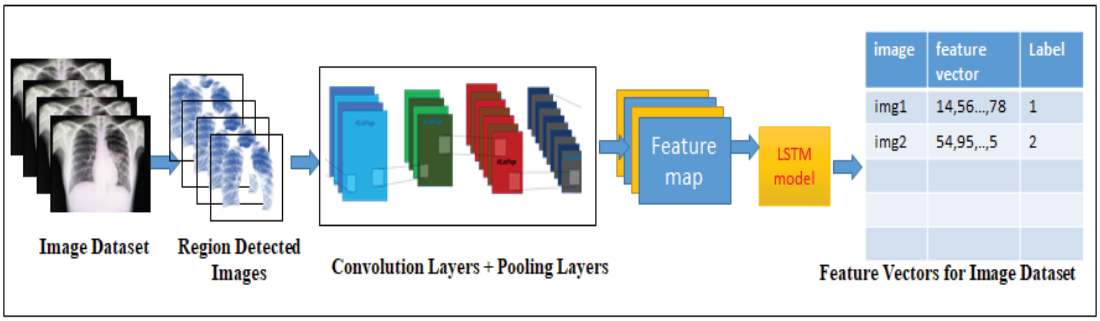

Figure 3. Flow of proposed feature extraction for chest X-ray image dataset

for the preprocessed image using a pre-trained conv-net and the rest is the generation of a feature vector using the LSTM model.

- **Extract feature map**. In this step, the preprocessed image is used as input and its RGB color spaces are used as the input for the input layers of pre-trained conv-net. The pre-trained Alex Net is used to extract the feature map of the input image.
- **Extract feature vector**. In this step, the LSTM model is used to model the extracted feature map to form the feature vector to symbolize the reasonable information of an image for the coming training step.

The characteristic retrieval procedure sequence is presented in Figure 3 in which the input is the image dataset consisting of chest X-ray images. The preprocessed images serve as inspiration for the projected feature process. The output of this step is the feature vectors that represent the image information efficiently.

2.4 Deep feature extraction

Convolution bases are typically utilized for feature extraction since they are more versatile than tightly coupled layers. Convolution bases can also be reused. Regardless of the computer-vision problem or any other problem, the feature maps of the conv-net are the presence maps of generic ideas across an image. It is not possible to extract features from tightly linked layers because they lose the ability to explain the position of objects in the input picture. Convolutional feature maps continue to represent the location of objects in densely connected layers. The deep features of an image are created using the extracted feature maps.

To accommodate the input layers of Alex Net, the input photos are shrunk to a 299x299 matrix size. From the initial grayscale picture, which has a pixel value range of 0 to 255, the RGB color space is produced. The representations that the previous network learned to extract the important features from fresh data are used in feature extraction in neural networks. As CNN has the deep transfer learning (DTL) property in feature extraction, the pre-trained Alex Net is employed in the

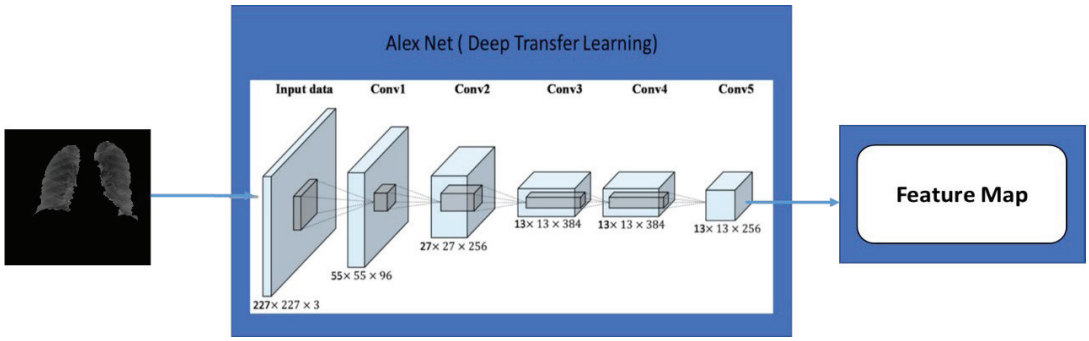

Figure 4. Feature Map Extraction of an image

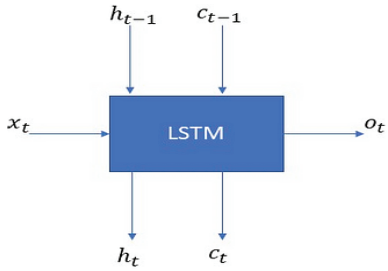

$$f_t = \sigma_g\,(W_f \times x_t + U_f \times h_{t-1} + b_f)$$
$$i_t = \sigma_g\,(W_i \times x_t + U_i \times h_{t-1} + b_i)$$
$$o_t = \sigma_g\,(W_o \times x_t + U_o \times h_{t-1} + b_o)$$
$$c'_t = \sigma_c\,(W_c \times x_t + U_c \times h_{t-1} + b_c)$$
$$c_t = f_t \cdot c_{t-1} + i_t \cdot c'_t$$
$$h_t = o_t \cdot \sigma_c(c_t)$$

f_t *is the forget gate*
i_t *is the input gate*
o_t *is the output gate*
c_t *is the cell state*
h_t *is the hidden state*

Figure 5. LSTM Model

proposed method to extract the deep features of an input. The 13x13x256 extracted feature maps are utilized as the deep features in an image. Eight layers make up the pre-trained Alex Net architecture: three fully linked layers and five convolutional layers.

- Without padding formula

– $\frac{n-f}{s} + 1 * \frac{n-f}{s} + 1$

- With padding formula

– $\frac{n+2p-f}{s} + 1 * \frac{n+2p-f}{s} + 1$

The flow of deep feature extraction for images is shown in following Figure 4.

2.5 LSTM model

The extracted feature maps model by Long Short-Term Memory (LSTM) to form a feature vector. LSTM can be used to model time series forecasting problems and LSTM is a recurrent neural network that can be used to a variety of sequential data with high levels of accuracy. In the work of Mohammad-Rahimi, et. al. (2021), the input data to LSTM was a three-dimensional array that was. Output Data of LSTM was a two-dimensional array. The LSTM model consists of time-step calculation for input data to model the data into relevant data representation. One time-step LSTM model is as follows:

One time-step input, output, and the equations for data representation are shown in Figure 5. The CNN output or the source string itself can both be used as the LSTM's input . The inputs from the preceding time-step LSTM are $h(t\text{-}1)$ and $c(t\text{-}1)$ and the result of the LSTM during that time-step is o(t). Additionally, the LSTM produces the c(t) and h(t) for use by the subsequent time period LSTM. Kumar *et al.* (2023) effectively applied the LSTM model with RSARM to propose a hybrid model combining for time series forecasting system.

Data in Figure 5 may only be calculated once; it must be computed again for the subsequent time step. The definition of 10-time phases in this work means that the preceding calculations will be calculated 10 times, once for every phase in the sequence of 10-time steps. The biases (b_f, b_i, b_o, b_c) and weight matrices ($W_f, W_i, W_o, W_c, U_f, U_i, U_o, U_c$) remain constant from one time period to the next. In this case, identical weight matrices are employed to calculate the results of many time steps.

2.6 Classification step and dataset

Support Vector Machine (SVM) is the name of a supervised machine learning technique. Since SVM provides a thorough solution for the categorization of the data, it has an advantage over other existing classification algorithms. Unlike other data categorization methods now in use, it develops a single hyper-plane worldwide to divide information sources into several groups. According to the work of Cristianini & Shawe-Taylor (2000), the flow of Support Vector Machines Classification is as follows.

Select support vector. Support vectors are observations corresponding to strictly positive estimates.

Training SVM. To find the maximum margin separator, we solve the following optimization problem:

$$\begin{aligned} &\boldsymbol{w}.\boldsymbol{x}^c + b > +1 \quad for\ positive\ cases \\ &\boldsymbol{w}.\boldsymbol{x}^c + b < -1 \quad for\ negative\ cases \\ &and \quad ||\boldsymbol{w}||^2 \ \ is\ as\ small\ as\ possible \end{aligned}$$

This is tricky but it's a convex problem. There is only one optimum and we can find it without fiddling with learning rates weight decay or early stopping. The optimization problem, it has been solved by quadratic programming. In quadratic programming, a polynomial kernel is used:

$$K(\boldsymbol{x}, \boldsymbol{y}) = (\boldsymbol{x}.\boldsymbol{y} + 1)^p$$

where the value of p is 2 in our classifier training and it takes time proportional to N^2 which is really bad for very big datasets.

Testing SVM: The separator is defined as the set of points for which:

$$\begin{aligned} &\boldsymbol{w}.\boldsymbol{x} + \boldsymbol{b} = \mathbf{0} \\ &\boldsymbol{so\ if} \quad \boldsymbol{w}.\boldsymbol{x}^c + \boldsymbol{b} > \mathbf{0} \quad \boldsymbol{say\ its\ a\ positive\ case} \\ &\boldsymbol{and\ if} \quad \boldsymbol{w}.\boldsymbol{x}^c + \boldsymbol{b} < \mathbf{0} \quad \boldsymbol{say\ its\ a\ negative\ case} \end{aligned}$$

Chowdhury *et al.* (2020), and Rahman, Chowdhury, & Khandakar (2021) contributed a free-to-use collection called COVID-19_

Table 1. Number of images in dataset

No.	Label	No. of images
1	COVID-19	3616
2	Viral Pneumonia	1345
3	Normal	10192
Total		**15153**

Radiography_Dataset images which has more than 10,000 chest X-ray images for COVID-19, Pneumonia, and Normal classes. Doctors have annotated the majority of the images in the collection. The development of freely available neural network algorithms that can precisely categorize COVID-19 illnesses for chest X-ray images is made possible by the increasing and maturing COVID-19 pictures database. All images have a resolution of 299x299 pixels and are stored as Portable Network Graphics (PNG) files. Table 1 displays the number of images for each label of Dataset.

3. Experiment and Performance Evaluation

By utilizing readily accessible ground truth-labeled datasets, evaluation was carried out in this study to indicate how correctly the classification task had been carried out. Comparable to analyzing labeling techniques used in machine learning and other research disciplines, the process of evaluating classification is comparable. On three distinct types of chest X-ray images, our system also assessed the suggested feature extraction and classification algorithms. K-fold cross-validation was used to accomplish the evaluation.

k-fold cross-validation divides the dataset into k sections and validates them 10 times. One subset is the training set, while the rest of the k-1 subsets form the test set each validation time. The average classification accuracy, training duration, and prediction speed for all k are calculated. To assess classifier performance, this k-fold cross validation calculates true positive and false positive rates. This study evaluates classifier performance using different k values. 2-5-10 are k values. Our lung disease categorization removes theoretical values because k-fold cross-validation is bias-free. Figure 6 shows 10-fold cross-validation for classifier assessment.

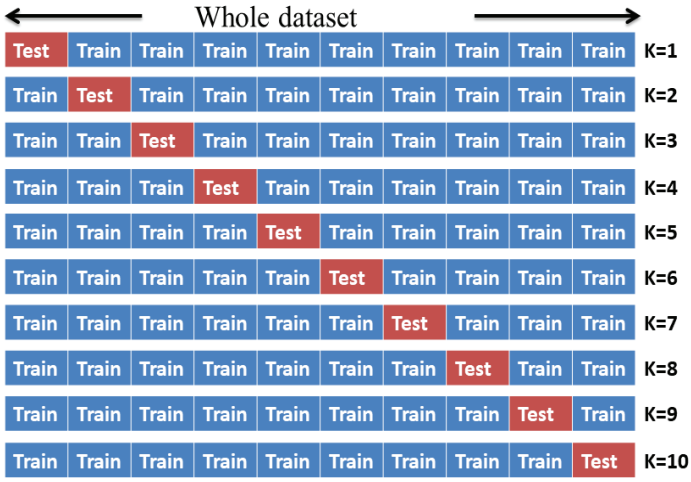

Figure 6. Partition of training and testing data in 10-fold cross validation

3.1 Classifier performance

By categorizing and assigning predefined names to untested or tested images, this research predicts the names of lung diseases. The accuracy of classification is predicted by the percentage of correct labels used by the trained classifier. In Chen *et al.* (2024), the classification equations for this system were computed accuracy, sensitivity, specificity, false positive rate, and false negative rate.

True Positive Rate. Sensitivity, recall, and percent of properly identified are other names for this. It gauges the proportion of positive labels that are really genuine labels. The ratio of properly recognized true labels over the total number of correctly categorized true and false cases is the value of sensitivity. The Sensitivity value ranges from 0 to 1. As described by Widmann (2019), the classifier's performance is greater if the sensitivity value is higher.

$$True\ Positive\ Rate = \frac{TP}{TP + FN}$$

where TP is the label that was correctly identified as true, and is the label that was wrongly classified as true.

False Negative Rate. The number of data that are mistakenly excluded as members of the class is measured by a statistic known as the missed rate. The value of specificity ranges from 0 to 1. The classifier's performance is worse as shown by the greater False Negative Rate value.

$$False\ Positive\ Rate = \frac{FN}{TP + FN}$$

where is the label that is correctly categorized as false and is the label that is wrongly categorized as negative.

Positive Predictive Value. This is also known as precision, and it assesses the proportion of relevant facts that are properly and incorrectly classified. A positive classifier

test result is more likely to be accurate if the PPV is high. The range of the positive predictive value is 0 to 1. A classifier with a greater Positive Predictive Value performs better.

$$Positive\ Predictive\ Value = \frac{TP}{TP + FP}$$

False Discovery Rate. This counts the number of wrong rejections among data that was properly and incorrectly categorized. The false negative rate has a value between 0 and 1. The classifier has better performance, according to the False Discovery Rate.

$$Positive\ Discovery\ Rate = \frac{FP}{FP + TP}$$

Accuracy. This is the proportion of samples that are accurately classified as having true or false labels. The accuracy value ranges from 0 to 1 in terms of probability and from 1 to 100 in terms of percentage. Higher accuracy numbers indicate a more accurate classifier.

$$Accuracy = \frac{TP + TN}{TP + FP + TN + FN}$$

3.2 A comparison of proposed and based frameworks

Deep features from based framework. As the CNN has the deep transfer learning (DTL) property in feature extraction, the pre-trained Alex Net is employed in the proposed method to extract the deep features of an input. The 13x13x256 extracted feature maps are utilized as the deep features in an image. A fully connected layer uses this feature map to create a feature vector with weighted learning rate factor 1 and bias learning rate factor 2 and the output size is 4096.

Deep features from proposed framework. The extracted deep feature (1x4096) is inputted into a flattened layer to convert the feature map into a sequence feature vector. Then LSTM model is used to model the deep feature into the feature vector to represent the image information effectively. In the LSTM model, the biases (b_f, b_i, b_o, b_c) matrix size is (900x1) and weight matrices ($W_f, W_i, W_o, W_c, U_f, U_i, U_o, U_c$) size are (900x225) with a number of hidden units 225. The size of the feature vector is 225. The comparison of classification accuracy for the based framework and proposed framework is presented in Table 2.

3.3 A comparison of proposed features and state-of-the-art features

The proposed features is compared with the Gray-Level Co-occurrence Matrix (GLCM) and the erosion feature ensemble (EFE).

- **GLCM**. Mall, Singh, & Yadav (2019) recommended the use of GLCM for image detection and categorization for Chest X-ray images. The function $P(i, j, d)$ is used to represent the GLCM, where

Table 2. A comparison of classification accuracy for proposed and based frameworks

Image	No. of Images	Labels	Deep Feature	Classification Accuracy	True Positive Rate	False Negative Rate	Positive Predictive Value	False Discovery Rate
Chest X-ray	15153	3	Proposed Framework	98.8%	95.3%	4.7%	97.6%	2.4%
			Based Framework	96.5%	94.4%	5.6%	93.5%	6.5%

Table 3. A comparison of classification accuracy for proposed and based frameworks

Image	No. of Images	Labels	Deep Feature	Classification Accuracy	True Positive Rate	False Negative Rate	Positive Predictive Value	False Discovery Rate
Chest X-ray	15153	3	Proposed Framework	98.8%	95.3%	4.7%	97.6%	2.4%
			GLCM	72.5%	70.4%	29.6%	69.5%	30.5%
			EFE	83.3%	81.7%	18.3%	83.1%	16.9%

i stands for the (x, y) gray level of the location and i represents the gray level of the pixel that is d pixels away from the place and a direction. The values in their investigation are 0, 45, 90, and 135 with $d = 1$. The feature vector for the GLCM texture feature has 36 dimensions.

- **EFE**. Neumann *et al.* (2014) proposed to use the amalgamation of gradient magnitude LBPs (Gmag LBP) and RGB color channels along with erosion band texture descriptors with $d = 1$. There are 112 dimensions in the feature vector (EFE). The comparison of classification accuracy for the proposed feature and other features is presented in Table 3.

By using a quadratic Support Vector Machine (SVM) classifier and 10-fold cross validation, we were able to accomplish our comparative findings. Pneumonia and Normal chest X-ray images were utilized in COVID-19 experiments to compare several aspects. Additionally, combinations of all chest X-ray images were used to demonstrate the database reliability of the benefits of our suggested feature. The suggested feature is contrasted with GLCM and EFE in this experiment. The suggested feature had greater classification accuracy than the competition, and the experiment's results for its true positive rate

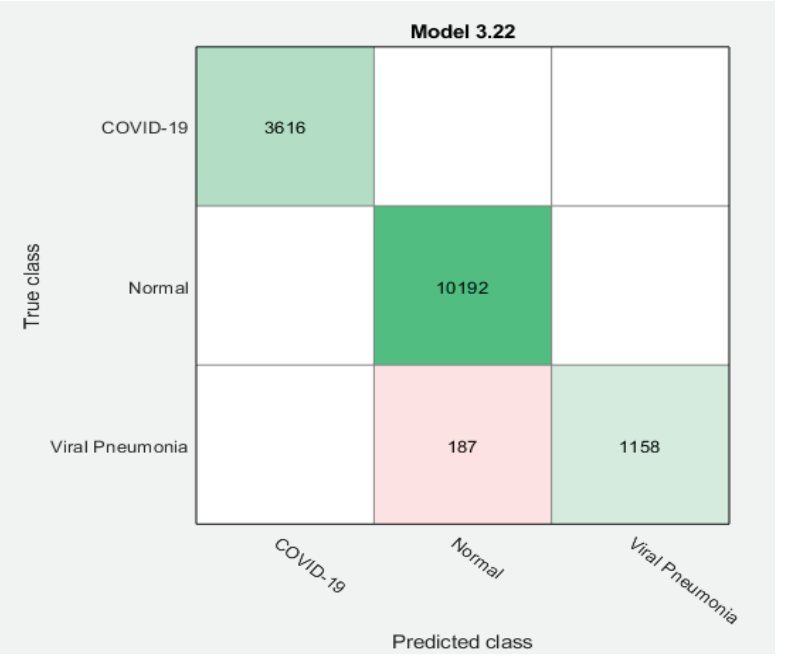

Figure 7. Confusion matrix of overall classification results in 10-fold cross-validation

were acceptable. To simplify the detailed results for the classification accuracy of the proposed feature, confusion matrix for classification results of proposed feature is presented in Figure 7. The confusion matrix now shows summary rows underneath the table. Positive predictive values are shown in green for the correctly predicted points in each class, and false discovery rates are shown below it in red for the incorrectly predicted points in each class.

4. Results and Discussion

In this experiment, using the chest X-ray images data set, the top row of Figure 7 shows all chest X-ray images with true class COVID-19. The columns show the predicted classes. In the top row, 100% of the chest X-ray images from COVID-19 are correctly classified, and also 100% for Normal diseases are correctly classified but the 86% of Viral Pneumonia diseases are correctly classified. Therefore, overall classification accuracy is 98.8% and 95.3**%** is the true positive rate for correctly classified points in this class, shown in the green cell in the True Positive Rate column of Figure 8.

The other chest X-ray images in the Viral Pneumonia row are misclassified: 14% of the chest X-ray images are incorrectly classified as from Normal, and 86% are correctly classified as Viral Pneumonia. 14% is the false negative rate for incorrectly classified points in this class, shown in the red cell in the False Negative Rate column of Figure 8. Although the false negative rate is 14%, the overall false negative rate is 4.7% and the overall classification accuracy of our proposed

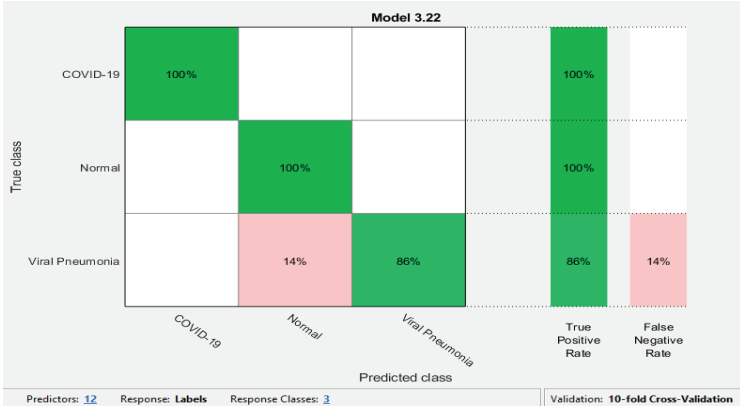

Figure 8. Confusion matrix of True Positive Rate and False Negative Rate results in 10-fold cross-validation

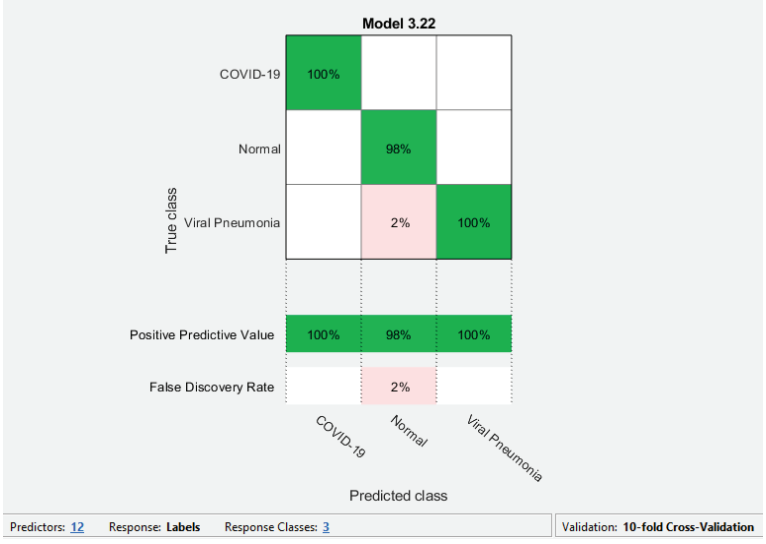

Figure 9. Confusion matrix of Positive Predictive Value and False Discovery Rate results in 10-fold cross-validation

framework is acceptable we also need to try to get a more effective true positive rate and less false negative rate.

As shown in Figure 9, a column-normalized column summary displays the percentages of correctly and incorrectly classified observations for each predicted class. For Covid19 and Viral Pneumonia labels, all of chest X-ray images are correctly classified. But for predicted label of Normal observations, 2% of Normal observations are misclassified as shown in the red cell of Figure 9. Therefore, the overall Positive Predictive Value is 97.6% with 2.4% of False Discovery Rate in this 10-fold cross validation. Although, the false negative rate is 14%, the overall false negative rate is 4.7% and the overall classification accuracy of our proposed framework is acceptable, but we also need to try to achieve a more effective true positive rate and less false negative rate.

5. Limitations

Our proposed system is only intended for the lung disease classification system and the input image must be a chest X-ray image. The background of the input image must be gray color and not complex. In the future, the focus of image pre-processing will be on performing operations on lung disease images with various backgrounds. A mobile application will be developed to serve as a real-time system for the recognition of lung diseases.

6. Conclusions

Diagnosing lung disorders is a c hallenging task in the field of medicine. Accurately classifying lung diseases is essential for medical advancement and aiding professionals. This problem is addressed by applying image processing techniques to chest X-ray images to identify lung diseases. For the identification of lung diseases, we present a novel model-based feature derivation approach that uses the deep features (Feature map) and LSTM models. We conducted an experiment using the COVID-19_Radiography_Dataset images to demonstrate the invariance of our suggested characteristics to scale and lighting. Although the features we suggest is typical, it makes a trade-off between classification accuracy and training duration. Although our suggested features can accurately model the deep features and be used to recognize lung disorders, we still need to work with and explore other image-processing techniques to enhance our proposed features. Additionally, the proposed framework will be used for a system to detect lung disease, which may aid in and support a serious danger to people's health. For further extension, we also need to develop and implement other sequential models that have a better distribution than the LSTM model to model the deep features with a more efficient representation of the feature vector. Although our research has acceptable classification accuracy, we need to develop other statistically based or semantical features to represent image information more effectively for classification. In the future, the classification of lung diseases will likely involve the consideration of a combination of symptoms specific to the lung region to achieve a higher level of accuracy in classification.

Acknowledgments

I wish to express my profound gratitude to Dr. Thu Zar Aung, ProRector of the University of Technology in Yatanarpon Cyber City, who is my supervisor. Without her excellent suggestions, guidance, consideration, and constant support, this research paper would not have been possible.

References

Alshmrani, G. M. M., Ni, Q., Jiang, R., Pervaiz, H., & Elshennawy, N. M. (2023). A deep learning architecture for multi-class lung diseases classification using chest X-ray (CXR) images. *Alexandria Engineering Journal*, 64, 923-935. https://doi.org/10.1016/j.aej.2022.10.053

Bhosale, Y. H. & Patnaik, K. S. (2023). PulDi-COVID: Chronic obstructive pulmonary (lung) diseases with COVID-19 classification using ensemble deep convolutional neural network from chest X-ray images to minimize severity and mortality rates. *Biomedical Signal Processing and Control*, 81, 104445. https://doi.org/10.1016/j.bspc.2022.104445

Chen, Z, *et al.* (2024). A novel imbalanced dataset mitigation method and ECG classification model based on combined 1D_CBAM-autoencoder and lightweight CNN model. *Biomedical Signal Processing and Control*, 87(Part B), 105437. https://doi.org/10.1016/j.bspc.2023.105437

Chowdhury, M. E. H. *et al.* (2020). Can AI help in screening viral and COVID-19 pneumonia?. *IEEE Access*, 8, 132665-132676. https://doi.org/10.1109/ACCESS.2020.3010287

Cristianini, N. & Shawe-Taylor, J. (2000). An Introduction to Support Vector Machines and Other Kernel-Based Learning Methods. Cambridge University Press, Cambridge, UK. https://doi.org/10.1017/CBO9780511801389

Kanjanasurat, I., Tenghongsakul, K., Purahong, B., & Lasakul, A. (2023) CNN-RNN network integration for the diagnosis of COVID-19 using chest X-ray and CT images. *Sensors*, 23(3), 1356. https://doi.org/10.3390/s23031356

Khan, A. A., Madendran, R. K., Thirunavukkarasu, U., & Faheem, M. (2023a). D^2PAM: Epileptic seizures prediction using adversarial deep dual patch attention mechanism. *CAAI Transactions on Intelligence Technology*, 8(3), 755-769. https://doi.org/10.1049/cit2.12261

Khan, A. A., Shahid, M. M. A., Bashir, R. N., Iqbal, S., Shahid, A. Sh. A., Maqbool, J., & Wechtaisong, C. (2023b). Detection of omicron caused pneumonia from radiology images using convolution neural network (CNN). *Computers, Materials & Continua*, 74(2). 3743-3761. https://doi.org/10.32604/cmc.2023.033924

Kujur, A., Raza, Z., Khan, A. A. & Wechtaisong, C. (2022). Data complexity based evaluation of the model dependence of brain MRI images for classification of brain tumor and Alzheimer's disease. *IEEE Access*, 10, 112117-112133. https://doi.org/10.1109/ACCESS.2022.3216393

Kumar, B., Sunil, & Yadav, N. (2023). A novel hybrid model combining βSARMA and LSTM for time series forecasting. *Applied Soft Computing*, 134, 110019. https://doi.org/10.1016/j.asoc.2023.110019

Mall, P. K., Singh, P. K., & Yadav, D. (2019). "GLCM based feature extraction and medical X-RAY image classification using machine learning techniques". Proceeding of the IEEE Conference on Information and Communication Technology (CICT), IEEE, Allahabad, India, December 6-8, 2019, 1-6. https://doi.org/10.1109/CICT48419.2019.9066263

Mohammad-Rahimi, H., Nadimi, M., Ghalyanchi-Langeroudi, A., Taheri, M., & Ghafouri-Fard, S. (2021). Application of machine learning in diagnosis of COVID-19 through X-ray and CT images: A scoping review. *Frontiers in Cardiovascular Medicine*, 8, 638011. https://doi.org/10.3389/fcvm.2021.638011

Neumann, M., Hallau, L., Klatt, B., Kersting, K., & Bauckhage, C. (2014). Erosion band features for cell phone image based plant disease classification. Proceeding of 22nd International Conference on Pattern Recognition (ICPR), IEEE, Stockholm Sweden, August, 24-28, 2014, 3315-3320. https://doi.org/10.1109/ICPR.2014.571

Ouyang, X. *et al.* (2020). Dual-sampling attention network for diagnosis of COVID-19 from community acquired pneumonia. *IEEE Transactions on Medical Imaging*, *39(8)*, 2595-2605. https://doi.org/10.1109/TMI.2020.2995508

Rahman, T., Chowdhury, M., & Khandakar, A. (2021). COVID-19 Radiography Database. Retrieved 10 February 2023. Retrieved from https://www.kaggle.com/datasets/tawsifurrahman/covid19-radiography-database

Rahman, T. *et al.* (2021). Exploring the effect of image enhancement techniques on COVID-19 detection using chest X-ray images. *Computers in Biology and Medicine*, 132, 104319. https://doi.org/10.1016/j.compbiomed.2021.104319

Sharifrazi, D. *et al.* (2021). Fusion of convolution neural network, support vector machine and Sobel filter for accurate detection of COVID-19 patients using X-ray images. *Biomedical Signal Processing and Control,* 68, 102622. https://doi.org/10.1016/j.bspc.2021.102622

Tomar, D., & Agarwal, S. (2015). A comparison on multi-class classification methods based on least squares twin support vector machine. *Knowledge-Based Systems*, 81, 131-147. https://doi.org/10.1016/j.knosys.2015.02.009

Vishnoi, V. K., Kumar, K., Kumar, B., Mohan, S., & Khan, A. A. (2023). Detection of apple plant diseases using leaf images through convolutional neural network. *IEEE Access*, 11, 6594-6609. https://doi.org/10.1109/ACCESS.2022.3232917

Wang, D., Mo, J., Zhou, G., Xu, Liang, & Liu, Y. (2020). An efficient mixture of deep and machine learning models for COVID-19 diagnosis in chest X-ray images. *PLoS ONE* 15(11), e0242535. https://doi.org/10.1371/journal.pone.0242535

Widmann, M. (2019). *Let's talk confusion matrix and class statistics*. Retrieved 16 March 2023. Retrieved from https://www.knime.com/blog/from-modeling-to-scoring-confusion-matrix-and-class-statistics

Xia, T., Fu, X., Fulham, M., Wang, Y., Feng, D., & Kim, J. (2023). CT-based radiogenomics framework for COVID-19 using ACE2 imaging representations. *Journal of Digital Imaging*, 2023. https://doi.org/10.1007/s10278-023-00895-w